PAPER ID: 1198
DOI: 10.18462/iir.gl.2020.1198

Thermal Characteristics in Supercritical CO2 Along Heating Tube

Takuya TAZAWA[(a)], Seiya YOSHIDA[(b)], Haruhiko YAMASAKI[(c)], Hiroyuki WAKIMOTO[(d)], Hiroshi YAMAGUCHI[(e)], Takeshi KAMIMURA[(f)], Kazuhiro HATTORI[(g)], Petter NEKSA[(h)]

[(a)] Doshisha University
Kyotanabe-shi, 610-0394, Japan, cyjd1503@mail4.doshisha.ac.jp
[(b)] Doshisha University
Kyotanabe-shi, 610-0394, Japan, ctwc0604@mail4.doshisha.ac.jp
[(c)] Osaka Prefecture University
Sakai-shi, 599-8531, Japan, hyamasaki@me.osakafu-u.ac.jp
[(d)] Doshisha University
Kyotanabe-shi, 610-0394, Japan, ctwd0605@mail.doshisha.ac.jp
[(e)] Doshisha University
Kyotanabe-shi, 610-0394, Japan, hyamaguc@mail.doshisha.ac.jp
[(f)] Mayekawa mfg. co., LTD
Koto-ku, 135-8482, Japan, takeshi-kamimura@mayekawa.co.jp
[(g)] Mayekawa mfg. co., LTD
Koto-ku, 135-8482, Japan, kazuhiro-hattori@mayekawa.co.jp
[(h)] NTNU
Trondheim, NO-7465, Norway, petter.neksa@sintef.no

ABSTRACT

The system using CO_2 as a refrigerant such as heat pump or Rankine cycle, depends greatly on the phase state and physical properties of CO_2. In the present study, as a basic research on CO_2 in the supercritical state, an experiment using a plane heating tube has been conducted, where two peaks of the local heat transfer coefficient are confirmed along the tube length. It is thought that the Prandtl number and the Reynolds number influence each peak. It is still unknown, however, how the carbon dioxide in the supercritical state flows internally. In the present study, thermal flow characteristics of supercritical state CO_2 by reproducing internal flow with numerical calculation is also conducted. From both experiment and numerical verification, it is revealed that the local heat transfer along the pipe length is greatly affected by the changes of CO_2 properties at (or after) the pseudo-critical state.

Keywords: Solar Rankine System, CO_2, Supercritical Fluid, Solar Energy, Numerical Analysis.

1. INTRODUCTION

CO2 is in a supercritical state at a temperature of 304.3 K and a pressure of 7.38 MPa. When CO2 enters the supercritical state, various physical properties change rapidly. In particular, the specific heat capacity is remarkably increased, and a large amount of heat can be carried. Against the background of the above, a supercritical CO2 solar Rankine System (SCRS) that uses solar thermal energy as a heat source and CO2 as a working fluid has been proposed, and research with optimized operation in mind. Has been done [1], [2]. SCRS is a system that can simultaneously recover electrical energy and thermal energy from solar energy, and consists of four components: a heat collecting part, a power generating part, a heat exchanging part, and a driving part. In the heat collecting section consisting of a vacuum tube type solar collector, CO2 absorbs solar heat in the process of flowing and becomes high temperature and high pressure. Output is obtained during the process of CO2 expansion in the power generation section consisting of a turbine or expander. Heat energy is recovered in the heat exchange section consisting of a heat exchanger, and CO2 is liquefied. Finally, it is a

closed loop system in which CO2 liquefied by the drive unit consisting of a feed pump is sent again to the solar collector.

Since SCRS uses CO2 as the refrigerant, it depends greatly on the phase state and physical properties of CO2 in the system, and is thought to affect the heat recovery characteristics. Therefore, research on the characteristics investigation and optimization of the heat collecting part has been conducted in the past [3]-[5]. Among them, the peculiar reaction that the peak of the local heat transfer coefficient expressed by the following formula changes with the heat input is shown.

$$h_x = Q \cdot \left\{ A\left(T_{1W} - T_b\right) \right\}^{-1} \quad \text{Eq. (1)}$$

Where, Q is the heat input, A is the cross-sectional area, T_{IW} is the wall temperature, and T_b is the bulk temperature. It was thought that the Prandtl number and Reynolds number affected, respectively. However, since the supercritical state is high pressure, it is difficult to know how CO2 in the supercritical state flows inside by a visualization experiment. Therefore, in this study, numerical calculation was performed for the purpose of reproducing the flow inside the heating tube.

2. COMPUTATIONAL FLUID DYNAMICS

2.1. Governing equation

The inlet velocity of the computational model in this study is considered to be very low compared to the sound velocity. Therefore, in this calculation, SLAU2 [6], which is called the full velocity scheme, is used to calculate the inviscid flux. A detailed description of SLAU2 will be given later.

It is conducted that the following three equations as the governing equations: continuity equation, momentum equation, and energy equation.

$$\partial \boldsymbol{Q}/\partial t + \partial \boldsymbol{F_k}/\partial x_k = \partial \boldsymbol{F_{vk}}/\partial x_k \quad \text{Eq. (2)}$$

$$Q = \rho \boldsymbol{i} + \left(\rho u_l\right)\boldsymbol{j} + \left(\rho E\right)\boldsymbol{k} \quad \text{Eq. (3)}$$

$$F_k = \left(\rho u_k\right)\boldsymbol{i} + \left(\rho u_l u_k + p\delta_{uk}\right)\boldsymbol{j} + \left(\rho u_k H\right)\boldsymbol{k} \quad \text{Eq. (4)}$$

$$\boldsymbol{F_{vk}} = \left(\tau_{lk}\right)\boldsymbol{j} + \left(u_m \tau_{mk} + \lambda \cdot \partial T/\partial x_k\right)\boldsymbol{k} \quad \text{Eq. (5)}$$

$$\tau_{lk} = \mu\left(\partial u_l/\partial x_k + \partial u_k/\partial x_l\right) - 2/3 \cdot \mu\delta_{lk} \cdot \partial u_n/\partial x_n \quad \text{Eq. (6)}$$

Equation (2) is the conserved amount, equation (3) is the inviscid flux, equation (4) is the viscous flux, and equation (5) is the viscous stress. Where t is time in s, ρ is density in $kg.m^{-3}$, u is velocity in $m.s^{-1}$, p is pressure in Pa, μ is viscosity in Pa.s, and λ is thermal conductivity in $W.(m.K)^{-1}$, and T represent temperature in K. The following constitutive equations are used to solve these governing equations. Speed is calculated by following equation (7) from the momentum m and the density ρ.

$$m = \rho u \quad \text{Eq. (7)}$$

For the temperature T, first calculate the internal energy e in $J.kg^{-1}$ from the total energy E.

$$e = E/\rho - 1/2 \cdot |u|^2 \quad \text{Eq. (8)}$$

The enthalpy h in $J.kg^{-1}$ is calculated using the internal energy e.

$$h = e + p/\rho \quad \text{Eq. (9)}$$

Once the enthalpy h is obtained, the temperature can be calculated as $T = T(p, h)$ because the temperature is a function of the enthalpy h and the pressure p. The relationship between the CO2 enthalpy h at temperature T

This is the accepted version of http://dx.doi.org/10.18462/iir.gl.2020.1198

and the pressure p at CO2 is calculated using the thermophysical property database PROPATH. Similarly, viscosity μ and thermal conductivity λ is calculated by using PROPATH.

2.2. Inviscid flux method SLAU2

For the calculation of the inviscid flux in this study, a solution method called the full velocity scheme was used. As the name implies, the full-speed scheme is a scheme that can solve problems in a wide range of speeds, and can perform stable calculations even in the low-speed range, which is difficult for density-based systems. In recent years, such a calculation method has been devised especially in the field of space engineering, and one of them is the velocity division method called SLAU2.

SLAU2 is a calculation method that was developed as an extension of the Flux Vector Splitting method, and calculates the information flowing into the cell from the characteristic speed. In this SLAU2, the numerical flux is derived from the following equation.

$$\boldsymbol{F} = \boldsymbol{\psi}^{+}\left(\dot{m}+\left|\dot{m}\right|\right)/2 - \boldsymbol{\psi}^{-}\left(\dot{m}+\left|\dot{m}\right|\right)/2 + \tilde{\boldsymbol{p}}\boldsymbol{N} \qquad \text{Eq. (10)}$$

$$\boldsymbol{\psi} = \left(1,\quad u_x,\quad u_y,\quad H\right)^T \qquad \text{Eq. (11)}$$

$$\boldsymbol{N} = \left(0,\quad n_x,\quad n_y,\quad 0\right)^T \qquad \text{Eq. (12)}$$

The mass flux m and the pressure flux p included in Eq. (2.9) are obtained by the following equations.

$$\dot{m} = \left\{\rho_L\left(V_{nL}+\left|\bar{V}_n\right|^{+}\right)+\rho_R\left(V_{nR}-\left|\bar{V}_n\right|^{-}\right)-\Delta p\cdot\chi/\bar{c}\right\}/2 \qquad \text{Eq. (13)}$$

$$\tilde{p} = \left(p_L+p_R\right)/2+\left(P^{+}+P^{-}\right)\cdot\left(p_L-p_R\right)/2+\left(P^{+}+P^{-}-1\right)\cdot\bar{\rho}\bar{c}\sqrt{\left(u_L{}^2+u_R{}^2\right)/2} \qquad \text{Eq. (14)}$$

Where, each variable is obtained from the following formula.

$$\left|\bar{V}_n\right|^{+} = (1-g)\left|\bar{V}_n\right| + g\left|V_{nL}\right| \qquad \text{Eq. (15)}$$

$$\left|\bar{V}_n\right|^{-} = (1-g)\left|\bar{V}_n\right| + g\left|V_{nR}\right| \qquad \text{Eq. (16)}$$

$$\left|\bar{V}_n\right| = \left(\rho_L\left|V_{nL}\right|+\rho_R\left|V_{nR}\right|\right)/\left(\rho_L+\rho_R\right) \qquad \text{Eq. (17)}$$

$$g = -\max\left[\min\left(M_L,\quad 0\right),\quad -1\right]\cdot\min\left[\max\left(M_R,\quad 0\right),\quad 1\right] \qquad \text{Eq. (18)}$$

$$\chi = \left(1-\hat{M}\right)^2 \qquad \text{Eq. (19)}$$

$$\hat{M} = \min\left(1,\quad \sqrt{\left(u_L{}^2+u_R{}^2\right)/2}\Big/\bar{c}\right) \qquad \text{Eq. (20)}$$

$$M = V_n/\bar{c} = (u\cdot n)/\bar{c} \qquad \text{Eq. (21)}$$

$$P^{\pm} = \left(1\pm\mathrm{sign}\left(M\right)\right)/2,\quad \text{if}\left|M\right|\geq 1 \qquad \text{Eq. (22-1)}$$

$$P^{\pm} = \left(M\pm 1\right)^2\cdot\left(2\mp M\right)/4,\quad \text{otherwise} \qquad \text{Eq. (22-2)}$$

Where, the subscripts L and R indicate the values on the left and right of the cell boundary, and + and-indicate the values on the left and right of the cell boundary. n is the surface normal direction of the cell, c is the speed of sound, and M is the Mach number. g is a switching function to the complete upwind scheme, and sign() is a sign function that returns +1, 0, -1 depending on the sign of the argument. max() and min() are functions that compare two arguments and return a large value and a small value, respectively.

2.3. Higher spatial accuracy

In order to perform the above SLAU2 calculation, the value at the boundary of the calculation cell is required. It is possible to use the center of the calculation cell as the representative point and use that value as the value at the boundary as it is, but in that case the spatial accuracy will be first-order accuracy. In order to improve the accuracy, it is possible to consider the distribution function in the calculation cell and interpolate the

This is the accepted version of http://dx.doi.org/10.18462/iir.gl.2020.1198

boundary value from that function. The method is called MUSCL interpolation [7], and the following equation is the equation. U indicates the value to be interpolated, and in this case it is the conserved amount or the basic amount. The subscript i means the cell number.

$$U_{i+1/2} = U_i + \left\{(1-\kappa)\phi(r_i)(U_i - U_{i-1}) + (1+\kappa)(U_{i+1} - U_i)\phi/r_i\right\} \quad \text{Eq. (23)}$$

Where, κ is a parameter of MUSCL interpolation, and the accuracy can be controlled by the value. In this calculation, the third-order accuracy (κ = 1/3) was always used. Also, ri in the formula represents the ratio of the gradients of adjacent cell values and is given by the following formula. Φ is the flow velocity limiting function.

$$r_i = (U_i - U_{i-1})/(U_{i+1} - U_i) \quad \text{Eq. (24)}$$

The spatial accuracy of the calculation is improved by the above MUSCL interpolation, but at the same time, the calculation becomes unstable near a large gradient. Since the value overshoots as it is and may swell up to infinity and the calculation may end, the following formula called the minmod flow velocity limiting function was introduced. This is a function that changes the spatial accuracy by detecting the gradient that makes the calculation unstable.

$$\min\mathrm{mod}(a,\ b) = \left\{\mathrm{sign}(a) + \mathrm{sign}(b)\right\}/2 \cdot \min\left(|a|,\ |b|\right) \quad \text{Eq. (25)}$$

Where, a and b are expressed as follows.

$$a = U_{i+1} - U_i \quad \text{Eq. (25-1)}$$

$$b = U_i - U_{i-1} \quad \text{Eq. (25-2)}$$

In addition, the viscous flux expressed by Eq. (4) is calculated by the central difference.

2.4. Time integration

In this numerical calculation, time integration was performed using the following two-stage Runge-Kutta method. In the equation, n and n + 1 mean the number of time steps, and n + 1/2 means half the time step.

$$\phi^{n+1/2} = \phi^n + \Delta t/2\left(t^n,\ \phi^n\right) \quad \text{Eq. (26-1)}$$

$$\phi^{n+1} = \phi^n + \Delta tf\left(t^{n+1/2},\ \phi^{n+1/2}\right) \quad \text{Eq. (26-2)}$$

2.5. Method of calculating physical properties of CO2 by PROPATH

In this study, thermophysical properties such as enthalpy and density of CO2 are required for system evaluation and heat collection characteristic evaluation. However, since it is impossible to directly obtain these physical property values, it is necessary to use the measurable physical property values such as pressure and temperature to calculate by the equation of state. In this study, the thermophysical property calculation software called PROPATH (A Program Package for Thermophysical Properties of Fluids) v13.1[8] was used to calculate these physical property values. PROPATH has a built-in equation of state for calculating each thermophysical property value by the study of S. Angus et al. [9], and each thermophysical property value can be calculated from measurable physical property values.

2.6. Results and Discussion

The calculation results are shown in Figure 1. The figure shows the magnitude of the temperature at 5 seconds, 10 seconds, 15 seconds, and 20 seconds and the magnitude of velocity in the x-axis direction at 5 seconds, 10 seconds, 15 seconds, and 20 seconds. The left end is the inlet and the right end is the outlet. The image on the right is a color bar showing the numerical size and color target. Figure 2 shows a graph of the local heat transfer coefficient derived from the results related to the temperature field. Here, the local heat transfer coefficient is expressed by Eq. (1).

This is the accepted version of http://dx.doi.org/10.18462/iir.gl.2020.1198

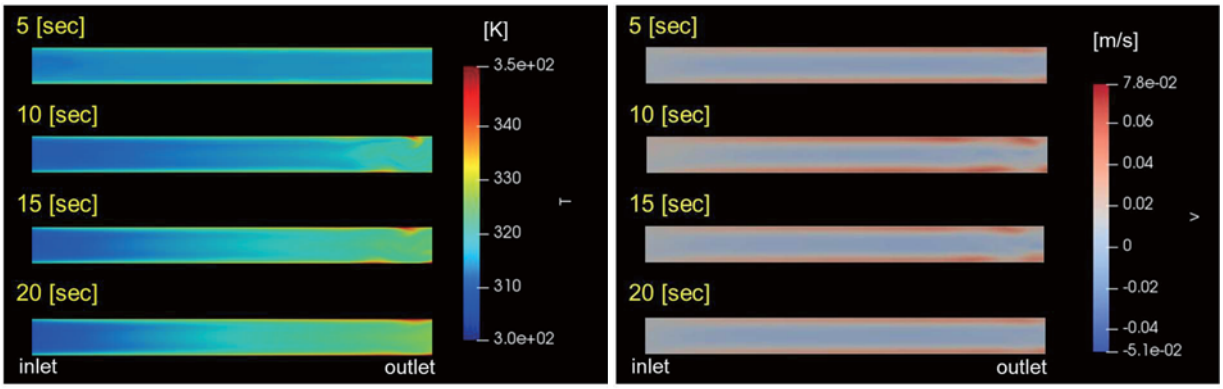

Figure 1: Temperature field (Left) and Velocity field (Right) (5 sec ~ 20 sec)

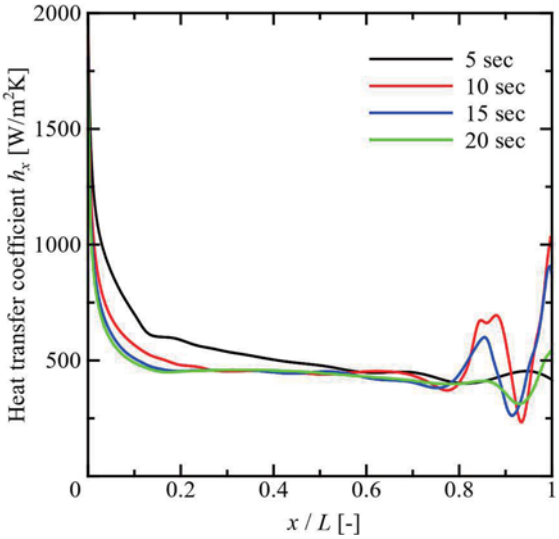

Figure 2: Heat transfer coefficient

2.6.1. Simulation by SLAU2

From the results in Figure 1, the calculation method using SLAU2 to derive the inviscid flux did not stop because the numerical values diverged to infinity during the calculation. Focusing on the calculation period (t = 0 to 20 sec), the evidence of overshoot and its increase is not seen from the results at t = 20 sec. Therefore, it can be said that the use of SLAU2 was successful in terms of computational stability. Similar upper and lower surface heating two-dimensional channel flow was calculated using another scheme. However, considering that the calculation stopped due to divergence immediately after the start of calculation, this calculation scheme is relatively stable for supercritical fluids. It turns out that the flow can be analysed.

2.6.2. Regarding disturbance

From Figure 1, it can be seen that the flow is disturbed when looking at the rear part of the calculation results. Let us consider the cause of this disturbance.

Looking at the results for the local heat transfer coefficient in Figure 2, it can be seen that the local heat transfer coefficient is greatly disturbed by the flow disturbance. If this calculation is correct, it may qualitatively indicate that the disturbance formed a peak in heat transfer coefficient. However, looking at the local heat transfer coefficient over time, it can be seen that after the peak peaks at t = 10 sec, the peak gradually falls until t = 20 sec. From this, the bounce may occur in the rear part of the computational domain.

2.6.3. Regarding local heat transfer coefficient

Looking at the diagram for the local heat transfer coefficient in Figure 2, a peak can be seen at the rear of the calculation region, as mentioned earlier. Considering that this is due to the reflected wave, the result at t = 20 sec is the result of this calculation. Therefore, looking at these results, it can be seen that the local heat transfer

This is the accepted version of http://dx.doi.org/10.18462/iir.gl.2020.1198

coefficient at the inlet becomes infinite due to the inlet effect, and thereafter, the local heat transfer coefficient decreases with heating and becomes almost constant. There is no large peak as seen in the experiment. Looking at the temperature field results in Figure 1, it can be seen that the pseudocritical state is reached near the wall. In addition, the local heat transfer coefficient slightly increases at the dimensionless distance of 0.3. From the above, it is considered that the first peak is obtained by calculation.

3. CONCLUSIONS

A two-dimensional channel flow was calculated using SLAU2 to derive the inviscid flux. As a result, it is obtained that the calculation is relatively stable. And, it is observed that the first peak in numerical analysis by reproducing the pseudocritical state of CO_2.

NOMENCLATURE

p	pressure (Pa)	m	mass flux($kg \times m^{-2} \times s^{-1}$)
T	temperature (K)	u	velocity ($m \times s^{-1}$)
ρ	density ($kg \times m^{-3}$)	t	time (s)
μ	viscosity (Pa×s)	λ	heat transfer coefficient ($W \times m^{-1} \times K^{-1}$)
e	internal energy ($J \times kg^{-1}$)	E	total energy ($J \times kg^{-1}$)
h	enthalpy ($J \times kg^{-1}$)		

REFERENCES

The sources should be presented as follows:

[1] H. Yamaguchi, X.R. Zhang, K. Fujima, M. Enomoto, N. Sawada, Solar energy powered Rankine cycle using supercritical CO2, Applied Thermal Engineering 26, (2006), 2345-2 354

[2] X.R. Zhang, H. Yamaguchi, D. Uneno, K. Fujima, M. Enomoto, N. Sawada, Analysis o f a novel solar energy powered Rankine cycle for combined power and heat generation using supercritical carbon dioxide, Renewable Energy 31 (2006) 1839-1854.

[3] X.R. Zhang, H. Yamaguchi, D. Uneno, Experimental study on the performance of solar Rankine system using supercritical CO2, Renewable Energy 32 (2007) 2617-2628.

[4] X.R. Zhang, H. Yamaguchi, An experimental study on evacuated tube solar collector using supercritical CO2, Applied Thermal Engineering 28 (2008) 1225-1233.

[5] Chayadit Pumaneratkul, Yuhiro Iwamoto and Hiroshi Yamaguchi, Nozzle test to Supercritical CO2 turbine in Rankine cycle system, International Journal of Advances in Science and Technology, ISSN 2348-5426, pp.167-174(2015).

[6] Kitamura Keiichi, Assessment of SLAU2 and Other Flux Functions with Slope Limiters in Hypersonic Shock-Interaction Heating, Computers & Fluids, Vol.245, 2013, pp.62-83.

[7] B. van Leer, Towards the ultimate conservative difference scheme IV, A new approach to numerical convection, Journal of Computational Physics, 23, 276- 299 (1977).

[8] PROPATH GROUP, PROPATH version 13.1, (2008).

[9] S.Angus, B.Armstrong and K.M.de Reuck, International Thermodynamic Table of the Fluid State-3 Carbon Dioxide,(IUPAC,3,1976).

This is the accepted version of http://dx.doi.org/10.18462/iir.gl.2020.1198